J. Phase Equilib. Diffus. (2021) 42:441–451
https://doi.org/10.1007/s11669-021-00908-7

Investigation on the Phase Relationship and Solidification Processes of Mg-rich Mg-Mn-Y Alloys

Tao Chen[1,2] · Liling Mo[1,2] · Yuan Yuan[1,2] · Jiawei Liu[1,2] · Jun Wang[1,2] · Dajian Li[3] · Bin Jiang[1,2] · Fusheng Pan[1,2]

Submitted: 14 January 2021 / in revised form: 25 June 2021 / Accepted: 9 July 2021 / Published online: 28 July 2021

Abstract Information of solidification processes, liquidus temperatures, and phase relationship of the Mg-Mn-Y system in the Mg-rich corner was systematically studied using differential scanning calorimetry (DSC) measurement, x-ray diffraction (XRD) analysis and scanning electron microscope (SEM) analysis. One single-phase region (Hcp), two two-phase-equilibrium regions (Hcp + Cbcc & Hcp + $Mg_{24}Y_5$), and one three-phase-equilibrium region (Hcp + Cbcc + $Mg_{24}Y_5$) were identified in the Mg-rich corner at 550 °C in this work. No ternary phase was observed within the currently studying composition range. Corresponding calculations using the current available thermodynamic description of the Mg-Mn-Y system for the comparison with experimental results were performed. The experimental and calculation results show certain deviations in the phase transition temperatures and the tie-lines of the equilibrium phase regions. The differences are attributed to the extreme low concertation of alloying elements alloyed in Mg in this work, where few studies were performed in literature and nevertheless included in the previous assessment work. Therefore, the current results could provide an essential basis for the further study and revision of the thermodynamic description of the Mg-Mn-Y system and the design/development of new alloy and process of Mg-Mn-Y based alloys.

Keywords Mg-Mn-Y system · phase-equilibrium · solidification process · thermodynamic calculation

1 Introduction

With the increasing demand for environmental protection and energy-saving, magnesium (Mg) alloys, as the lightest structural material, have attracted extensive attention in the transportation and 3C fields,[1–3] as well as the energy application field.[4,5] However, the broad applications of Mg alloys are still limited due to the poor plasticity property at room temperature and poor corrosion-resistance property. To improve these properties of Mg alloys, some methods have been developed, such as alloying,[6–9] rapid solidification and processing,[10,11] coating,[12,13] etc. Among them, the alloying approach is the most vital method to improve the performance of Mg alloys. Many works have indicated that manganese (Mn) can significantly refine the microstructure and simultaneously enhance the strength and ductility[14–17] and also purify the melt of Mg alloys.[18,19] Moreover, with further Rare-earth (RE) elements addition, Mg-Mn-RE alloys have been reported to be able to provide improved creep resistance and an excellent combination of castability and toughness.[20,21] To also control the materials' cost for industrial application, those RE elements with lower prices are more attractive for Mg-Mn-RE alloys. Yttrium (Y), as a common rare earth element (RE) with an acceptable price, has become a promising alloying element in Mg-Mn alloys and

✉ Yuan Yuan
yuanyuan17@cqu.edu.cn

1 National Engineering Research Center for Magnesium Alloys, College of Materials Science and Engineering, Chongqing University, Chongqing 400000, People's Republic of China

2 State Key Laboratory of Mechanical Transmissions, College of Materials Science and Engineering, Chongqing University, Chongqing 400000, People's Republic of China

3 Karlsruhe Institute of Technology, Institute for Applied Materials – Applied Materials Physics (IAM-AWP), 76344 Karlsruhe, Germany

Table 1 Chemical compositions of the investigated alloys analyzed by XRF (Error $< \pm 0.03$ at.%)

Alloy	Chemical composition, at.%			Alloy	Chemical composition, at.%		
	Mg	Mn	Y		Mg	Mn	Y
MMY1	Bal.	0.37	0.31	MMY6	Bal.	0.18	4.06
MMY2	Bal.	0.30	0.47	MMY7	Bal.	1.46	2.89
MMY3	Bal.	0.67	0.49	MMY8	Bal.	0.99	3.43
MMY4	Bal.	0.21	1.32	MMY9	Bal.	0.39	6.31
MMY5	Bal.	0.64	1.52	MMY10	Bal.	0.26	7.11

has attracted many studies. It is found, the Mg alloys with the addition of Mn and Y possess an improved creep resistance, as well as a good combination of strength and ductility.[22,23]

Phase diagram and thermodynamic information of materials can provide fundamental information for alloys' behavior and processing.[24–27] Thus, it is necessary to understand the phase equilibrium and relationship of the Mg-Mn-Y system, which is essential for new alloy design and development. Studies on the phase diagram of Mg-Mn-Y alloys started as early as the 1970s. Sviderskaya et al.[28, 29] studied isothermal sections of Mg-rich Mg-Y and Mn-Mn-Y phase diagrams at different temperatures (200, 300, 400, 500 °C) by combining thermal analysis, microstructural investigation, electrical resistivity and microhardness measurements. No ternary compound was reported in their work. Drits et al.[30] made a brief summary of these data. Pisch et al.[31] investigated the phase equilibrium and microstructure of Mg-4Mn-1Y (wt.%) alloy by combining thermodynamic calculations and experiments. Giovannini[32] also studied the isothermal section at 500°C and his results were in good agreement with the results reported by Sviderskaya,[29] in respect of the vertical section and the four isothermal sections. However, the solubility of Mn and Y in Hcp reported by these two studies do not fit very well. In addition, by combining DTA, EDS analysis of key alloys, Antion[33] has a thermodynamic assessment of Mg-Mn-Y-Gd system. And, Kang et al.[34] had an assessment on the Mg-Ce-Mn-Y system and they also noted that there is quite a few experimental data of the Mg-Mn-Y system. Further, the isothermal section of the Mg-rich Mg-Mn-Y phase diagram at 550 °C hasn't been studied.

It is no doubt that the phase diagram of the Mg-rich Mg-Mn-Y system is essential for practical applications. Hence, the current work focuses on solidification processes and the phase relationship of Mg-Mn-Y alloys in the Mg-rich corner Mg-Mn-Y system, which can provide essential information for the design of Mg-rich Mg-Mn-Y alloys.

2 Experimental and Calculation Methods

2.1 Alloy Preparation

High purity Mg pieces (purity: 99.98 wt.%), Mg-15 wt.% Mn master alloy, and Mg-30 wt.% Y master alloy was used in the current work. Weighed starting materials were melted using a resistant furnace under the protective atmosphere of 99 vol.% CO_2 and 1 vol.% SF_6 in 211 stainless steel crucibles. The alloys were melted at $\sim$ 700 °C for 15 minutes and quenched in water with alloys in crucibles. Ten alloys, which compositions are located at the Mg-rich corner, were selected and prepared. Part of the ingots was isothermal heat-treatment by being buried in compacted graphite powder in cleaned stainless steel crucibles at 550 °C for 288 hours and finally quenched in cold water. The annealed samples were polished until the surface oxidations and contaminated layers have been removed clearly. An x-ray fluorescence spectrometer (XRF, XRF-1800) was used to measure the obtained chemical compositions of annealed samples, as listed in Table 1. The compositions of samples MMY2 and MMY9 have been measured three times using XRF. Their atomic percent of Mn in MMY2 and MMY9 is 0.30/0.30/0.30, 0.47/0.47/0.47 and Y is 0.38/0.41/0.39, 6.31/6.30/6.30, respectively. It is shown the experimental uncertainty range for XRF measuring these samples is less than $\pm$ 0.03 at.%.

2.2 Sample Analysis

Differential scanning calorimetry (DSC) measurement was performed on the annealed Mg-Mn-Y alloys using Swiss METTLER Synchronous Thermogravimetric Analyzer (TGA/DSC 1/1100 SF). Disks with Φ3mm*2mm size were cut from each annealed sample, then polished to less 10 mg per one in weight. Al_2O_3 crucibles (Outer diameter: 6.8 mm, height: 4 mm) were employed for the DSC measurements. The calibration procedure has been performed by DSC analysis on pure Mg (99.98 wt.%) and pure Zn

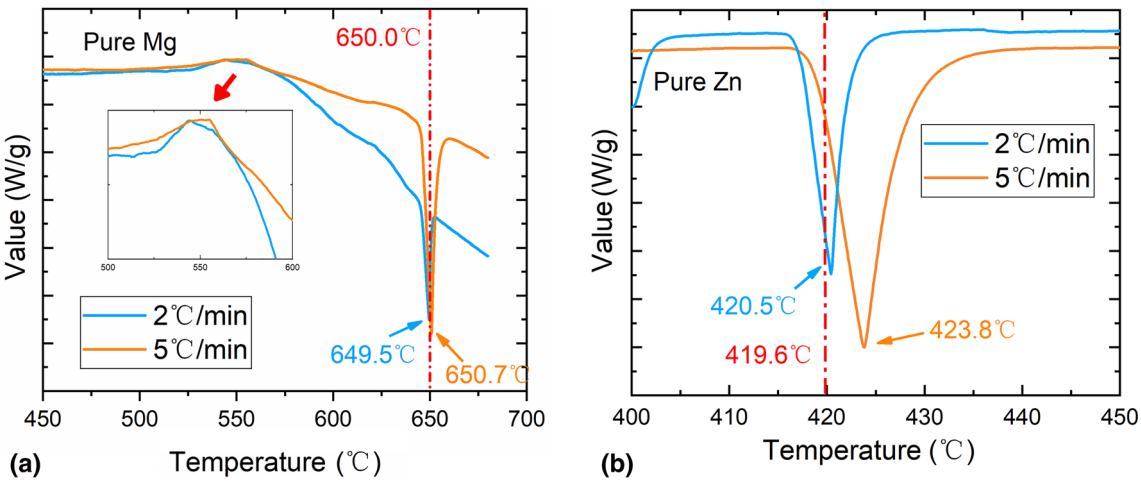

Fig. 1 The DSC results of (a) pure Mg and (b) pure Zn with the scanning rate of 5 °C/min and 2 °C/min

(99.8 wt.%) from 400 °C to 680 °C/450 °C with the scanning rate of 5 °C/min and 2 °C /min under the Argon atmosphere. The melting points of pure Mg and pure Zn are 650 °C[35] and 419.6 °C,[36] respectively. Our results are shown in Fig. 1 and it is seen the experimental errors for the melting points of these two pure metals are less than 5 °C. Therefore, for the DSC analysis in this work, the experimental uncertainty is ± 5 °C, which is acceptable for normal DSC analysis of the phase-transformation temperatures of the alloys. DSC measurements of Mg-Mn-Y alloys were performed from room temperature to 400 °C with the scanning rate of 10 °C/min and from 400 °C to 650–700 °C with the scanning rate of 5 °C/min. No higher temperatures were applied to avoid the high evaporation of Mg. The DSC results have been analyzed according to the work of Boettinger et al.[37]

Annealed samples were polished using the standard metallographic preparation method for metallurgic investigations. Ethanol was used as the cooling medium to avoid possible reactions with water. Later these samples were ultrasonically cleaned in ethanol solution for 5 minutes after polishing. Microstructural investigations were performed using scanning electron microscopy (SEM, TESCAN VEGA 3 LMH SEM) equipped with energy dispersive x-ray spectrometers (EDS). The acceleration voltage used for the EDS measurements is 20.0 kV.

Presented phases of the annealed samples were determined using the x-ray diffractometer (XRD, PANalytical Empyrean) with Cu x-ray at the voltage of 40 kV and current of 200 mA. 2θ between 5-90 deg, 2 deg per minute scan rate, and 0.02 deg step-size were applied. The combination of backscattered electron (BSE) micrographs, XRD patterns were used to determine phase relationships at 550 °C.

2.3 Calculation Method

The commercial software Pandat2013[38] and Thermo-Calc2019a[39] combined with their databases, PanMg2013 and TCMG5 were employed in this work. In simulating the solidification process and the relationships of phases, since all experiments are based on annealed samples, the equilibrium model was employed in the calculation work instead of the non-equilibrium model. In this work, the calculated results using the two databases were compared with the experimental results.

3 Results and Discussion

3.1 Thermal Analysis

The obtained chemical compositions of ten annealed samples have been listed in Table 1. Their DSC results have been shown in Figs. 2, 3, 4 and 5 and the detailed data has been listed in Table 2.

Figure 2 shows the DSC curves of the ten alloys studied in this work. All the DSC curves show one very distinct thermal effect, which corresponds to the melting point of the primary Mg phase (Hcp). The thermal effects of each curve, as shown in Fig. 5, were also labeled on the calculated isopleths (using PanMg database), where the dash line shows the composition of the corresponding alloy, and the different shapes show the temperatures of the different thermal effects. The liquidus temperatures and solidus temperatures of DSC results have also been marked in Fig. 6, the Mg-Y phase diagram. Detailed calculated results of phase transitions using PanMg database and that using TCMG database have been listed in Table 2 and compared with the current DSC results of Mg-Mn-Y system.

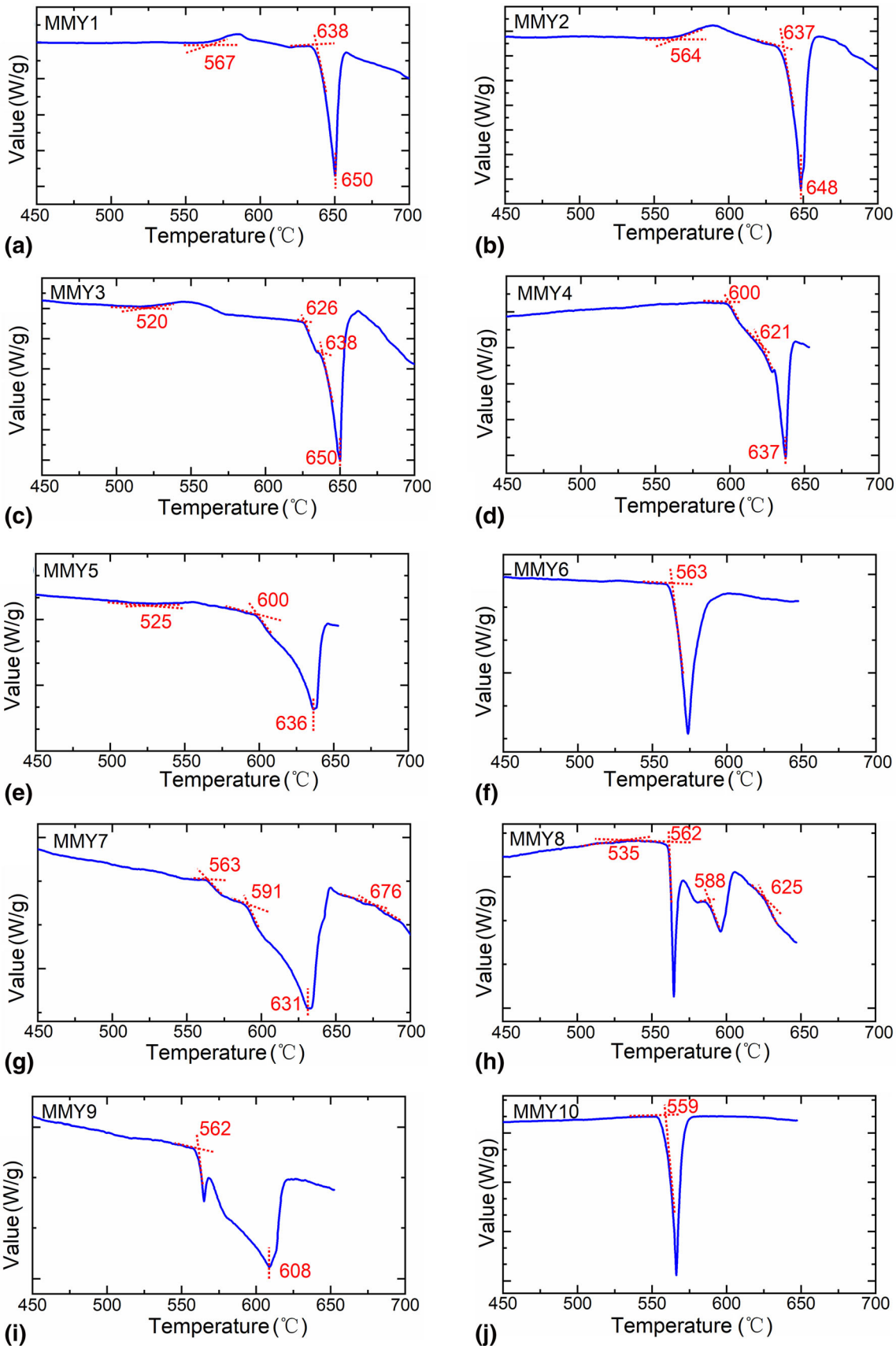
MMY1
638
567
650
Value (W/g)
450 500 550 600 650 700
Temperature (℃)
(a)
MMY2
637
564
648
Value (W/g)
450 500 550 600 650 700
Temperature (℃)
(b)
MMY3
626
520
638
650
Value (W/g)
450 500 550 600 650 700
Temperature (℃)
(c)
MMY4
600
621
637
Value (W/g)
450 500 550 600 650 700
Temperature (℃)
(d)
MMY5
600
525
636
Value (W/g)
450 500 550 600 650 700
Temperature (℃)
(e)
MMY6
563
Value (W/g)
450 500 550 600 650 700
Temperature (℃)
(f)
MMY7
563
591
676
631
Value (W/g)
450 500 550 600 650 700
Temperature (℃)
(g)
MMY8
562
535
588
625
Value (W/g)
450 500 550 600 650 700
Temperature (℃)
(h)
MMY9
562
608
Value (W/g)
450 500 550 600 650 700
Temperature (℃)
(i)
MMY10
559
Value (W/g)
450 500 550 600 650 700
Temperature (℃)
(j)

◀**Fig. 2** DSC heating curves of Mg-Mn-Y system with the heating run of 5 °C/min for (a) MMY1, (b) MMY2, (c) MMY3, (d) MMY4, (e) MMY5, (f) MMY6, (g) MMY7, (h) MMY8, (i) MMY9, (j) MMY10

As shown in Figs. 5 and 6, two thermal effects, referring to the solid-liquid transition process, were presented on the DSC curves of alloys MMY1, MMY2, MMY3, MMY4, and MMY5. The last thermal peak on each DSC curve well presents the corresponding liquidus point, and an adjoining small thermal effect shows the respective solidus point. The calculated results from two commercial databases are also close to our experimental results. The detailed values were listed in Table 2 and it is shown the experimentally measured temperatures and the calculated temperatures of liquid-containing reactions are close to each other. For example, the temperatures of liquidus of MMY1 shown from DSC, PanMg, TCMG results are 650, 648, 648 °C, respectively, and solidus points are 638, 639, 638 °C, respectively. For MMY6 and MMY10 alloys, there is only a thermal effect in this region. This thermal effect is corresponding to the eutectic reaction, L ↔ Hcp + $Mg_{24}Y_5$. And this thermal effect also can be observed in MMY7, MMY8, and MMY9 alloys. Sviderskaya and Padezhnova[29] reported that this reaction happens at 566°C in binary Mg-Y system. Our results of this reaction occurred at 563°C-559°C for these five alloys, which closed to the results of Sviderskaya and Padezhnova.[29] Furthermore, the thermal effects of MMY6, MMY9 and MMY10 happen at ∼ 562°C may be coming from the invariant reaction, L ↔ Hcp + $Mg_{24}Y_5$ + Cbcc (Complex body-centered crystal Mn). The calculated temperature of this invariant reaction is 572 °C for PanMg and 563 °C for TCMG, separately. Sviderkaya and Padezhnova[29] have reported that this reaction occurred at 535°C in the Mg-Mn-Y system. Antion[33] reported this reaction temperature is 577°C. Kang et al.[34] assessed the thermodynamic database of the Mg-Ce-Mn-Y system and they suggested that this value should be 566°C. In this work, the invariant reaction of L ↔ Hcp + $Mg_{24}Y_5$ + Cbcc occurred at 562°C for MMY9 alloy, closing to the calculated results of Kang et al.[34].

The exothermic reaction that happens at 530/560 °C may be attributed to the formation of MgO. The MgO may come from the reaction between Mg and Al_2O_3 crucibles or the reaction between Mg and a small amount of O_2 in the protective gas. To clarify this reaction, the samples pure Mg and MMY1 have been performed by DSC analysis using graphite crucibles. As shown in Fig. 3, these exothermic peaks also existed for samples in graphite crucibles. Therefore, Mg or Mg alloys may react with the trace O_2 existed in the Argon gas. The content of Y in samples MMY6 to MMY10 is higher than that of samples MMY1 to MMY5, which may provide the alloys better oxidation-resistance property[40] and then no obvious thermal effect has been observed. In addition, the invariant reaction for these alloys happens at ∼ 562 °C, which may cover this minor reaction. As shown in Fig. 4, these peaks only occurred in the first run and didn't affect the other reactions in the second run. Hence, this thermal peak is not considered in the description of the Mg-Mn-Y system.

However, there are still some differences between the current experimental results and the calculated results for the phase transition in the solid part. For example, the calculated results showed the formation temperatures of Mn(Cbcc) happens at 518, 494 and 595°C for the alloys named MMY1, MMY2, and MMY3, respectively. And the thermal effects of the formation of Cbcc are not observed in this work. These differences may be attributed to two

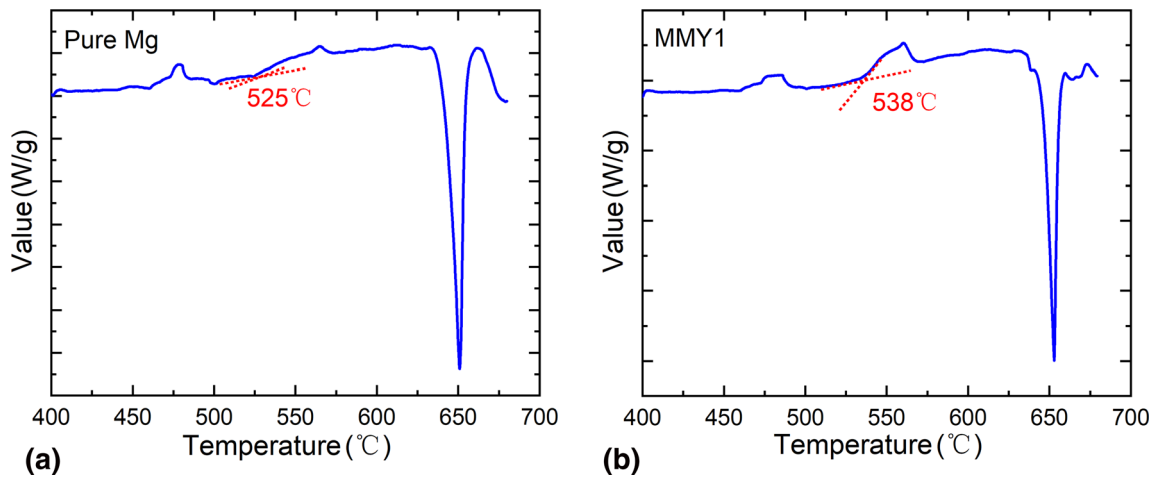

Fig. 3 The DSC results of (a) Pure Mg and (b) MMY1 with the scanning rate of 5 °C/min using graphite crucible.

Table 2 The transformation of Mg-Mn-Y alloys and their corresponding temperatures (Error $< \pm 5$ °C)

Alloy	Possible correspond reaction	Exp[a].	Pan2013	TCMG5
MMY1	Liquidus	650/647	648	648
	Solidus	638/639	639	638
	Cbcc formation		518	518
MMY 2	Liquidus	648/647	647	647
	Solidus	637/636	635	634
	Cbcc formation		494	494
MMY 3	Liquidus	650	647	647
	Solidus	626	635	632
	Cbcc formation		599	599
MMY 4	Liquidus	637	640	640
	Solidus	600	616	610
	Cbcc formation		461	460
MMY 5	Liquidus	636	639	639
	Solidus	600	611	603
	Cbcc formation		601	599
MMY 6	Liquidus		616	615
	Solidus		575	
	$Mg_{24}Y_5$ formation		562	
	Invariant reaction	563		566
	Cbcc formation		468	464
MMY 7	Cbcc formation	676		
	Liquidus	631	627	626
	Solidus	591	588	575
	Eutectic reaction	563		
	$Mg_{24}Y_5$ formation		482	469
MMY 8	Cbcc formation	625	661	636
	Liquidus	588	621	621
	Solidus		581	566
	Eutectic reaction	563		
	$Mg_{24}Y_5$ formation	535	521	539
MMY 9	Liquidus	608	593	592
	Invariant reaction	562	572	563
MMY 10	Liquidus		585	583
	Eutectic reaction		573	567
	Invariant reaction	559		
	Cbcc formation		550	546

Exp[a]: Heating run, T(°C), from 450 °C to 650 °C, 5 °C/min

Eutectic reaction: L ↔ Hcp + $Mg_{24}Y_5$

Invariant reaction: L ↔ Hcp + $Mg_{24}Y_5$ + Cbcc

possible reasons: (a) the current thermodynamic description of the Mg-Mn-Y system still needs to be improved with new experimental data imposed; (b) the thermal-effects of the precipitations that happen in named MMY1, MMY2, and MMY3 alloys are too small to be experimental detected precisely.

It has been reported that there is no ternary compound in the Mg-Mn-Y system and there is no Mn-Y compound in the Mg-rich corner of the Mg-Mn-Y system.[29]. Figure 6 shows our results that the temperature of liquidus and solidus of Mg-Y alloys with minor Mn addition have the same tendency as the Mg-Y system, which indicates that Mn element has little effect on the temperature of liquidus and solidus temperatures of Mg-Y-based alloy. Table 2 shows the temperature of L ↔ Hcp + Mg24Y5 + Cbcc ($\sim$ 562 °C) in the Mg-rich corner Mg-Mn-Y system is close to the temperature of L ↔ Hcp + Mg24Y5 ($\sim$ 563 °C) in Mg-Y system in this work. Zhou et al.[41] also

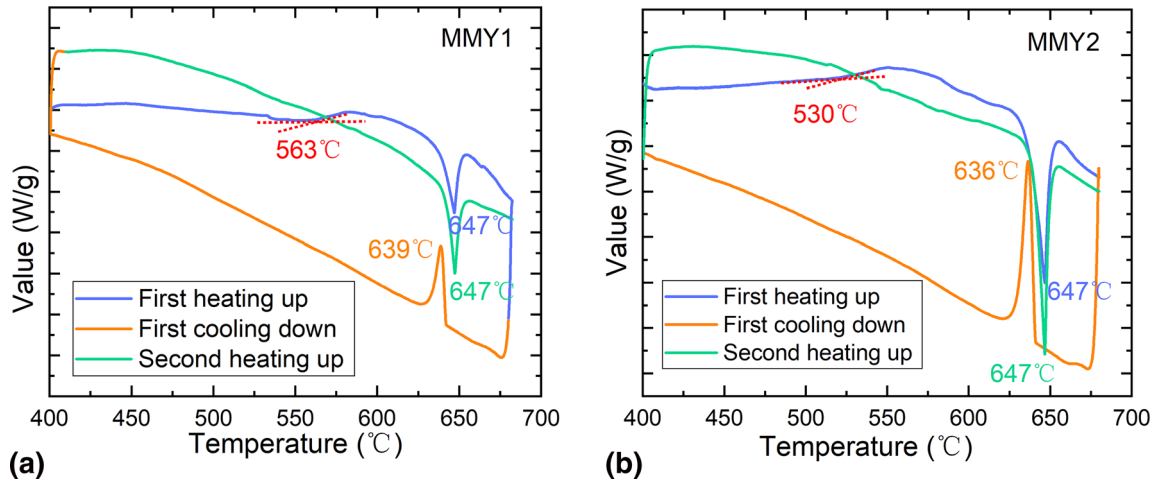

Fig. 4 The DSC results of (a) MMY1 with the scanning rate of 5 °C/min and (b) MMY2 with the scanning rate of 5 °C/min.

reported that the addition of Mn hardly affects the transition temperature and melting point of the Mg-Sr alloy.

In addition, there are also some differences in calculated results using two commercial databases, such as the formation temperature of $Mg_{24}Y_5$ for MMY8 and MMY9. Since there are few literature investigations on the dilute part of the phase diagram, the thermodynamic assessments in the dilute region should have low precision, or in other words, low reliability, which also brings differences in respect of different assessment works.

3.2 The Isothermal Section at 550 °C

Presented phases in the samples annealed at 550 °C for 288 hours were identified using XRD and shown in Fig. 7. Three phases, Hcp(Mg), Cbcc(Mn) and $Mg_{24}Y_5$, were observed in our alloys. Further, YH_2, which is easily formed in RE-containing alloys[42] but just got ignored in many reports, has been observed in the annealed alloys. Pisch et al.[31] also reported that the solution heat treatment leads to an unknown Y-rich phase in Mg-4Y-1Mn (wt.%) alloy, which is proposed to be YH_2 according to this work. In the following discussion, YH_2 was considered as an impurity phase and supposed to have no interaction with other phases. According to the XRD results, alloys MMY1, MMY2, and MMY4 consisted of Hcp, alloys MMY3, MMY5, MMY7 were composed of Hcp and Cbcc, and MMY6, MMY9, MMY10 were composed of Hcp and $Mg_{24}Y_5$. MMY8 was composed of Hcp, Cbcc and $Mg_{24}Y_5$. Figure 8 shows some examples of the backscattered electron images (BSE) for Mg-Mn-Y alloys. Figure 8a shows that MMY8 was composed of black matrix Hcp, blocky gray phase $Mg_{24}Y_5$ and light gray granular particles Cbcc. Figure 8b shows MMY9 was composed of Hcp and $Mg_{24}Y_5$, where a small amount of fine YH_2 particles were presented. No ternary phase was observed within the experimental composition range. One three-phase-equilibrium region of Hcp + $Mg_{24}Y_5$ + Cbcc has been observed.

The detected phases of the Mg-Mn-Y alloys (at the Mg-rich side) in this work and the predication of phases' compositions of these alloys by PanMg, TCMG have been listed in Table 3. The experimental results are in good agreement with most of the calculated data. But there were some differences between MMY8 and MMY9 alloys. The experimental results show MMY8 consisted of Hcp + Cbcc + $Mg_{24}Y_5$, but the calculated results show MMY8 consisted of Hcp + Cbcc. The MMY9 with 0.38 at.% Mn and 6.31 at.% Y was a three-phase region by calculated results, but the XRD and SEM results show that alloy was composed of Hcp and $Mg_{24}Y_5$.

The experimental results obtained in this work have added to the isothermal section of Mg-Mn-Y at 550 °C, as shown in Fig. 9. Shapes of different colors indicate the different alloys investigated in this work. Four regions were identified in the Mg-rich corner at 550 °C, including one single-phase region (Hcp), two two-phase regions (Hcp + Cbcc and Hcp + $Mg_{24}Y_5$) and one three-phase region (Cbcc + $Mg_{24}Y_5$ + Hcp), which agrees with the calculated results. However, the experimentally determined solubility of Mn in Mg(Hcp) of this work is a little bigger than that calculated. And the experimentally obtained tie-lines between Cbcc + Hcp phase region and the Cbcc + Hcp + $Mg_{24}Y_5$ phase region, as well as the Hcp phase region and Hcp + $Mg_{24}Y_5$ phase region in Mg-rich corner shifted a little downward in the results from TCMG than that from PanMg. There are some differences in the calculated results about the solubility of Y in Mg-Mn alloys at 550 °C in two commercial databases. The result from the solubility of Y in Mg-Mn alloys at 550 °C from TCMG is ~ 3.5 at.% and that form PanMg is ~ 3.85 at.%. Our results are more closing to the calculated results from TCMG. Okamoto assessed the Mg-Y system,[43,44] and the maximum solid

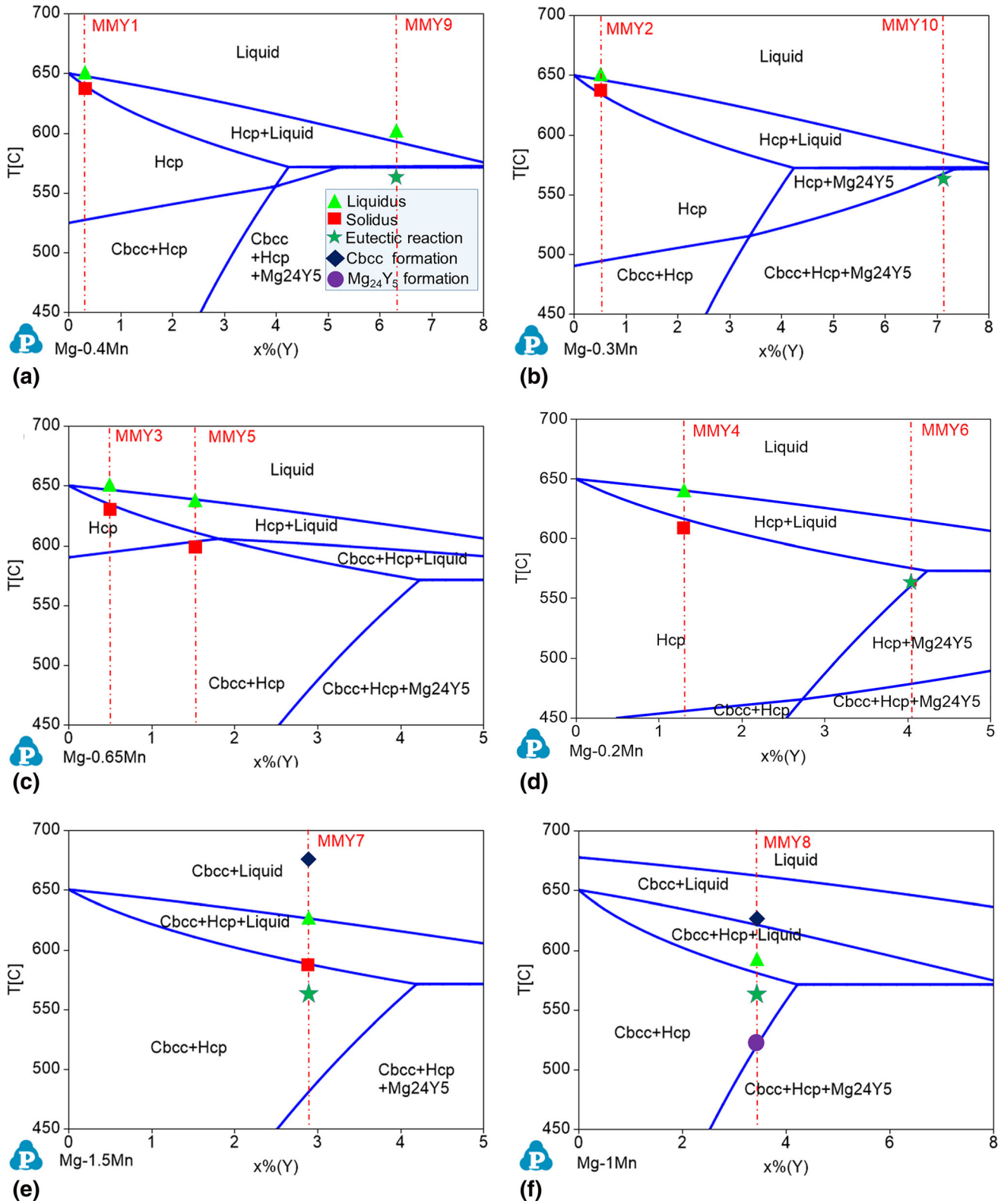

Fig. 5 Calculated vertical sections of Mg-Mn-Y system for (a) MMY1 and MMY9, (b) MMY2 and MMY10, (c) MMY3 and MMY5, (d) MMY4 and MMY6, (e) MMY7, (f) MMY8. The initial Mn-contamination of nominal value was taken for calculations in this figure, as shown in the lower-left corner of each sub-figure.

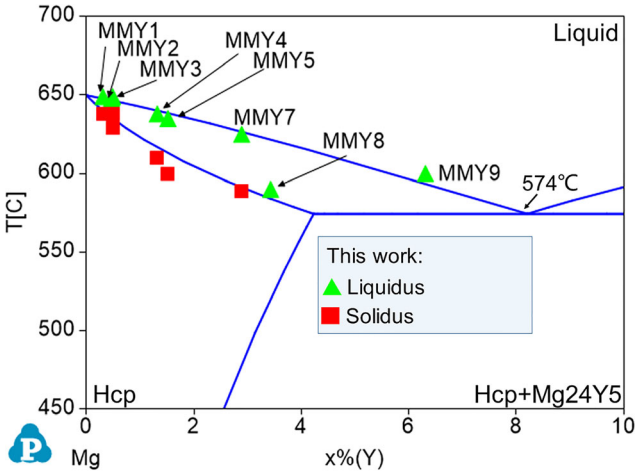

Fig. 6 Calculated vertical section of Mg-Y system.

solubility of Y in Mg(Hcp) is 3.4 at.% at 567 °C. Based on the current experimental results, the thermodynamic description of Mg-Mn-Y system in the Mg rich corner need more study.

4 Conclusion

This work investigated the phase relationship and thermodynamic equilibrium at the Mg-rich corner of the Mg-Mn-Y system by combining experiment analyses and thermodynamic calculations. Based on DSC, SEM and XRD analyses, the solidification sequences and phase transition temperature at the Mg-rich corner of the Mg-Mn-Y system were experimentally investigated. And the phase regions of the isothermal section at 550 °C in the Mg-rich

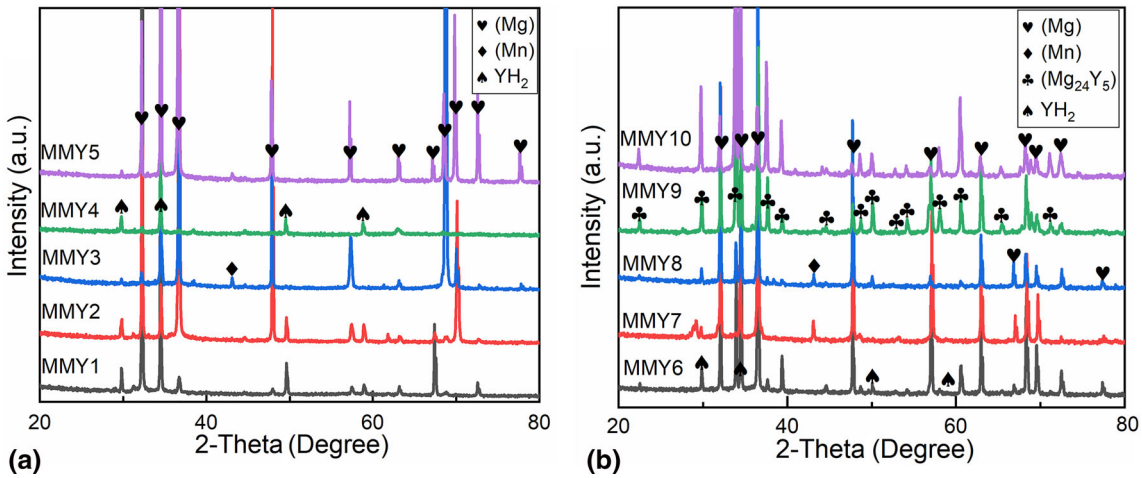

Fig. 7 XRD analysis of Mg-Mn-Y alloys for (a) MMY1 to MMY5; (b) MMY6 to MMY10

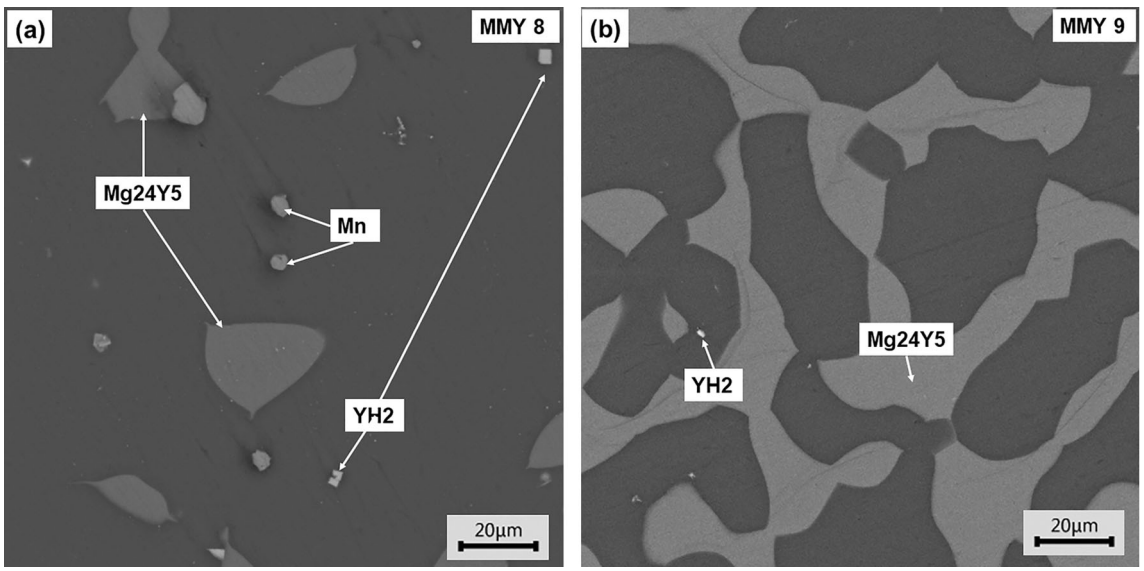

Fig. 8 BSE images of the Mg-Mn-Y alloys for (a) MMY8 ($Mg_{95.58}Mn_{0.99}Y_{3.43}$) and (b) MMY9 ($Mg_{93.31}Mn_{0.38}Y_{6.31}$)

Table 3 The detected phases of the Mg-Mn-Y alloys (at the Mg-rich side) in this work and the predication of phases' composition of these alloys by PanMg and TCMG

No.	Experimental Results			
	XRD	EDS	PanMg	TCMG
MMY1	Hcp	Hcp	Hcp	Hcp
MMY2	Hcp	Hcp	Hcp	Hcp
MMY3	Hcp + Cbcc	Hcp + Cbcc	Hcp + Cbcc	Hcp + Cbcc
MMY4	Hcp	Hcp	Hcp	Hcp
MMY5	Hcp + Cbcc	Hcp + Cbcc	Hcp + Cbcc	HCP + Cbcc
MMY6	Hcp + $Mg_{24}Y_5$	Hcp + $Mg_{24}Y_5$	Hcp + $Mg_{24}Y_5$	Hcp + $Mg_{24}Y_5$
MMY7	Hcp + Cbcc	Hcp + Cbcc	Hcp + Cbcc	Hcp + Cbcc
MMY8	Hcp + Cbcc + Mg24Y5	Hcp + Cbcc + $Mg_{24}Y_5$	Hcp + Cbcc	Hcp + Cbcc
MMY9	Hcp + $Mg_{24}Y_5$	Hcp + $Mg_{24}Y_5$	Hcp + Cbcc + $Mg_{24}Y_5$	Hcp + Cbcc + $Mg_{24}Y_5$
MMY10	Hcp + $Mg_{24}Y_5$	Hcp + $Mg_{24}Y_5$	Hcp + $Mg_{24}Y_5$	Hcp + $Mg_{24}Y_5$

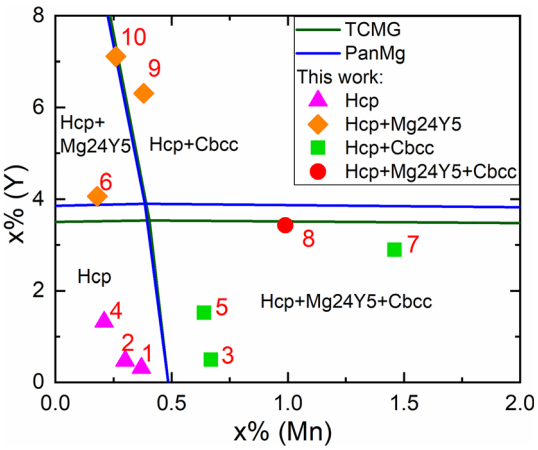

Fig. 9 Isothermal section of Mg-Mn-Y system at Mg-rich corner at 550 °C, shapes with different color represent experimental data points in the present experiment (Color figure online)

region were determined. There are some differences between the experimental results and the calculated results using the current databases, TCMG and PanMg. Current thermodynamic descriptions of the Mg-Mn-Y system need to be modified accordingly.

Acknowledgments The authors are grateful for the financial supports from Qinghai Provincial Science and Technology Key Program (No. 2018-GX-A1). The authors would like to thank joint lab for electron microscopy of Chongqing University.

References

1. J. Song, J. She, D. Chen, and F. Pan, Latest Research Advances on Magnesium and Magnesium Alloys Worldwide, *J. Magnes. Alloy*, 2020, **8**(1), p 1–41.
2. T. Xu, Y. Yang, X. Peng, J. Song, and F. Pan, Overview of Advancement and Development Trend on Magnesium Alloy, *J. Magnes. Alloy*, 2019, **7**(3), p 536–544.
3. J.P. Weiler, A Review of Magnesium Die-Castings for Closure Applications, *J. Magnes. Alloy*, 2019, **7**(2), p 297–304.
4. H. Yang, L. Wu, B. Jiang, W. Liu, J. Song, G. Huang, D. Zhang, and F. Pan, Clarifying the Roles of Grain Boundary and Grain Orientation on the Corrosion and Discharge Processes of α-Mg Based Mg-Li Alloys for Primary Mg-Air Batteries, *J. Mater. Sci. Technol.*, 2021, **62**, p 128–138.
5. D. Li, Y. Yuan, J. Liu, M. Fichtner, and F. Pan, A Review on Current Anode Materials for Rechargeable Mg Batteries, *J. Magnes. Alloy*, 2020, **8**(4), p 963–979.
6. J. Wu, Y. Yuan, X. Yu, T. Chen, D. Li, and e. al. , The High Temperature Oxidation Resistance Properties of Magnesium Alloys Alloyed with Gd and Ca, *J. Mater. Sci.*, 2020, **56**, p 8745–8761.
7. J. Wang, Y. Yuan, X.Y. Cheng, T. Chen, B. Jiang, D. Li, A. Tang, T. Boll, and F. Pan, The High-Solution Design of Magnesium Alloys, *Magnes. Technol.*, 2021, **2**, p 96.
8. C. Zhang, L. Wu, H. Liu, G.S. Huang, B. Jiang, A. Atrens, and F.S. Pan, Microstructure and Corrosion Behavior of Mg-Sc Binary Alloys in 3.5 wt.% NaCl Solution, *Corros. Sci.*, 2020, **174**, p 108831.
9. J. Zhao, B. Jiang, Y. Yuan, A. Tang, Q. Wang, T. Yang, G. Huang, D. Zhang, and F. Pan, Influence of Ca and Zn Synergistic Alloying on the Microstructure, Tensile Properties and Strain Hardening of Mg-1Gd Alloy, *Mater. Sci. Eng. A*, 2020, **785**, p 139344.
10. S. Yamaura, H. Kim, H. Kimur, A. Inoue, and Y. Arata, Electrode Properties of Rapidly Solidified Mg67Ni23Pd10 Amorphous Alloy, *J. Alloys Compd.*, 2002, **347**, p 239–243.
11. S. Zhou, X. He, P. Peng, T. Liu, G. Sheng, A. Tang, and F. Pan, Achieving High Yield Strength and Ductility in As-Extruded Mg-0.5Sr Alloy by High Mn-Alloying, *Materials*, 2020, **13**(18), p 1–13.
12. L. Wu, X. Ding, Z. Zheng, A. Tang, G. Zhang, A. Atrens, and F. Pan, Doublely-Doped Mg-Al-Ce-V2O74 LDH Composite Film on Magnesium Alloy AZ31 for Anticorrosion, *J. Mater. Sci. Technol.*, 2021, **20**, p 66–72.
13. J. Chen, L. Wu, X. Ding, Q. Liu, X. Dai, J. Song, B. Jiang, A. Atrens, and F. Pan, Effects of Deformation Processes on Morphology, Microstructure and Corrosion Resistance of LDHs

Films on Magnesium Alloy AZ31, *J. Mater. Sci. Technol.*, 2021, **21**, p 10–20.
14. T. Al-Samman, and X. Li, Sheet Texture Modification in Magnesium-Based Alloys by Selective Rare Earth Alloying, *Mater. Sci. Eng. A*, 2011, **528**(10–11), p 3809–3822.
15. X. Gu, Y. Zheng, Y. Cheng, S. Zhong, and T. Xi, In vitro Corrosion and Biocompatibility of Binary Magnesium Alloys, *Biomaterials*, 2009, **30**(4), p 484–498.
16. Z. Yu, A. Tang, J. He, Z. Gao, J. She, J. Liu, and F. Pan, Effect of High Content of Manganese on Microstructure, Texture and Mechanical Properties of Magnesium Alloy, *Mater. Charact.*, 2018, **136**, p 310–317.
17. Z. Yu, A. Tang, Q. Wang, Z. Gao, J. He, J. She, K. Song, and F. Pan, High Strength and Superior Ductility of an Ultra-Fine Grained Magnesium–Manganese Alloy, *Mater. Sci. Eng. A*, 2015, **648**, p 202–207.
18. T. Chen, X. Xiong, Y. Yuan, A. Tang, D. Li, A. Atrens, and F. Pan, Effect of Steels on the Purity of Molten Mg Alloys, *Adv. Eng. Mater.*, 2020, **8**, p 2000338.
19. T. Chen, Y. Yuan, T. Liu, D. Li, A. Tang, X. Chen, R. Schmid-Fetzer, and F. Pan, Effect of Mn Addition on Melt Purification and Fe Tolerance in Mg Alloys, *JOM*, 2021, **73**, p 892–902.
20. K.A.A.M. Celikin, and M. Pekguleryuz, Microstructure Investigation and the Creep Behavior of Mg-Sr-Mn Alloys, *Mater. Sci. Eng. A*, 2012, **550**, p 39–50.
21. E.T.B.L. Mordike, Magnesium Properties-Applications-Potential, *Mater. Sci. Eng. A*, 2001, **302**(1), p 37–45.
22. J. Grobner, and R. Schmid-Fetzer, Selection of Promising Quaternary Candidates from Mg-Mn-(Sc, Gd, Y, Zr) for Development of Creep-Resistant Magnesium Alloys, *J. Alloys Compd.*, 2001, **320**, p 296–301.
23. M. Yang, F. Pan, J. Shen, Y. Zhu, and C. Qin, Comparison about As-Cast Microstructures and Mechanical Properties of Mg-4Y-1.2Mn–0.9Sc and Mg–4Y–12Mn–1Zn (wt%) Magnesium Alloys, *J. Mater. Sci.*, 2010, **46**(9), p 3094–3100.
24. G.B. Olson, Designing a New Material World, *Science*, 2000, **288**(5468), p 993–998.
25. Y.A. Chang, S. Chen, F. Zhang, X. Yan, F. Xie, R. Schmid-Fetzer, and W.A. Oates, Phase Diagram Calculation: Past, Present and Future, *Prog. Mater Sci.*, 2004, **49**(3), p 313–345.
26. R. Shi, and A.A. Luo, Applications of CALPHAD Modeling and Databases in Advanced Lightweight Metallic Materials, *Calphad*, 2018, **62**, p 1–17.
27. D.S. Gandel, M.A. Easton, M.A. Gibson, and N. Birbilis, CALPHAD Simulation of the Mg–(Mn, Zr)–Fe System and Experimental Comparison with As-Cast Alloy Microstructures as Relevant to Impurity Driven Corrosion of Mg-Alloys, *Mater. Chem. Phys.*, 2014, **143**(3), p 1082–1091.
28. Z.A. Sviderskaya, and E.M. Padezhnova, Solid Solubility of Yttrium and Manganese in Magnesium, *Russ. Metall.*, 1970, **1**, p 137–140. (**in Russian**).
29. Z.A. Sviderskaya, and E.M. Padezhnova, Equilibria in Mg-Y and Mg-Y-Mn Systems, *Russ. Metall.*, 1968, **6**, p 126–130 (**in Russian**)..
30. M.E. Drits, E.M. Padezhnova, and T.B. Dobatkina, Physico-Chemical Interaction of the Elements in Mg-rich Alloys of the System Mg-Y-Me, *Magnesium Alloys*, Baikov Institute of Metallurgy, Moscow, 1978, p 74–78 (**in Russian**).
31. A. Pisch, C. Antion, C. Tassin, F. Baillet, J. Gröbner, and R. Schmid-Fetzer, Phase Equilibria, Microstructure and Properties of Novel Mg-Mn-Y Alloys, *Magnesium Alloys and their Applications*, K.U. Kainer, Ed., Wiley-VCH Verlag GmbH, Weinheim, 2006, p 98-102.
32. S.A. Giovannini M., Ferro R., Rogl P., Flandorfer H., Effenberg G., A Contribution to the Investigation of the Phase Relationship in the Mg-Mn-Y System, *Syntheses and Methodologies in Inorganic Chemistry,* 1995, **5**, p 538–542.
33. C. Antion, Etude du système Mg-Mn-Y-Gd et dévelopment d'alliages de magnésium pour des applications structurales á chaud, Ph.D. thesis, Institut National Polytechnique de Grenoble, 2003 (**in French**).
34. Y.-B. Kang, A.D. Pelton, P. Chartrand, P. Spencer, and C.D. Fuerst, Thermodynamic Database Development of the Mg-Ce-Mn-Y System for Mg Alloy Design, *Metall. Mater. Trans. A.*, 2007, **38**(6), p 1231–1243.
35. H. Okamoto, AI-Mg (Aluminum-Magnesium), *J. Phase Equilibria*, 1998, **19**, p 598.
36. J.L. Murray, The Al-Zn (Aluminum-Zinc) System, *Bull. Alloy Phase Diagr.*, 1983, **4**, p 55–56.
37. W.J. Boettinger, U.R. Kattner, K.W. Moon, J.H. Perepezko, DTA and Heat-flux DSC Measurements of Alloy Melting and Freezing, U.S. Government Printing office, 2006.
38. D.S.S.I. Chen, and F. Zhang, The PANDAT Software Package and its Applications, *Calphad*, 2002, **26**(2), p 175–188.
39. J.O. Andersson, T. Helander, L. Hdghmd, P. Shi, and B. Sundman, Thermo-Calc & Dictra, Computational Tools for Materials Science, *Calphad*, 2002, **26**, p 273–312.
40. X.M. Wang, X.Q. Zeng, Y. Zhou, G.S. Wu, S.S. Yao, and Y.J. Lai, Early Oxidation Behaviors of Mg–Y Alloys at High Temperatures, *J. Alloys Compd.*, 2008, **460**(1–2), p 368–374.
41. H. Zhou, C. Chen, Y. Wang, Y. Du, and S. Liu, Experimental Investigation and Thermodynamic Calculation of the Mg-Mn-Sr System, *Calphad*, 2016, **52**, p 110–119.
42. Y. Yuan, S. Delsante, J. Yi, and G. Borzone, A Revision of the Sm-rich Region of the Sm–Co System, *J. Alloys Compd.*, 2010, **508**(2), p 309–314.
43. H. Okamoto, Mg-Y (Magnesium-Yttrium), *J. Phase Equilib. Diff.*, 1992, **13**, p 105–106.
44. H. Okamoto, Mg-Y (Magnesium-Yttrium), *J. Phase Equilib. Diff.*, 2010, **31**(2), p 199–199.